Size-Dependent Oxygen Reduction Property of Octahedral Pt-Ni Nanoparticle Electrocatalysts

ARTICLE · OCTOBER 2014

DOI: 10.1039/C4TA04728A

3 AUTHORS, INCLUDING:

Changlin Zhang
University of Akron
10 PUBLICATIONS **53** CITATIONS

SEE PROFILE

Journal of Materials Chemistry A

PAPER

View Article Online
View Journal | View Issue

Cite this: J. Mater. Chem. A, 2014, 2, 19778

Size-dependent oxygen reduction property of octahedral Pt–Ni nanoparticle electrocatalysts

Changlin Zhang, Sang Youp Hwang and Zhenmeng Peng*

Received 11th September 2014
Accepted 7th October 2014

DOI: 10.1039/c4ta04728a

www.rsc.org/MaterialsA

The size effect on the electrocatalytic property of octahedral Pt–Ni alloy nanoparticles in the oxygen reduction reaction (ORR) was studied by making particles with different sizes and conducting electrochemical measurements. Octahedral Pt–Ni nanoparticles on carbon support (Pt–Ni/C) were produced using a facile and surfactant-free solid-state chemistry method. Two groups of octahedral Pt–Ni/C, including Pt_3Ni/C and $Pt_{1.5}Ni$/C, with particle size ranging from around 4 to 8 nm were prepared. Both the ORR activity and the stability of the two group catalysts were studied, which exhibited varying dependence over the particle size. The different relationships between the Pt–Ni size and the ORR property were investigated and attributed to alterations in the particle electronic/geometric structure and the Ni leaching behaviour.

Introduction

Electrocatalysts for the oxygen reduction reaction (ORR) has been an area of intensive research for decades because of both its fundamental complexity and practical importance for many applications, including polymer electrolyte membrane fuel cells (PEMFCs) and metal–air batteries.[1–4] The ORR activity and electrocatalyst stability are two difficulties which have been confronted in research.[5–9] The reaction, occurring by itself with very sluggish kinetics, needs the use of a good electrocatalyst to largely improve the rate. The harsh reaction conditions, *i.e.* high working potential and acidic electrolyte, imposes rigid requirements on the chemical stability of catalyst materials. Despite many efforts in researching non-precious materials, Pt remains the most effective element for both reaction kinetics and stability considerations.[10–14] Due to the high price of Pt and its insufficient activity, extensive studies have been devoted to decreasing Pt usage by exploring new Pt nanostructures with improved ORR property.[15–22] Many types of alloy, skin-layer, and core–shell structured electrocatalysts have been prepared and demonstrated with better ORR property compared to pure Pt.[2,23–30]

The studies on single crystalline Pt–Ni alloys reveal the importance of both catalyst composition and surface in affecting the ORR activity. Pt_3Ni (111) has been found to be the most active electrocatalyst compared to other composition/faceted Pt–Ni single crystals. It exhibits an exceptionally high activity of 18 mA cm^{-2} Pt at 0.9 V *vs.* RHE, which is about 90 times more active than the state-of-the-art Pt/C catalyst.[1] The dramatic improvement in the ORR kinetics using Pt_3Ni (111) has been attributed to its optimal electronic structure, with a down-shifted *d*-band center (ε_d) for surface Pt compared to pure Pt, and the (111) surface geometry. This finding has stimulated the research of octahedral Pt–Ni alloy nanoparticles, which have large specific (111) surfaces, as ORR electrocatalysts. However, big discrepancies in both the optimal Pt–Ni composition and the ORR activity exist between these nanoscale and bulk studies. For instance, Xia and co-workers synthesized octahedral Pt–Ni alloy nanoparticles with different compositions, among which 9 nm-$Pt_{2.4}Ni$ octahedrons were found to be the most active in ORR and exhibited 7.0 mA cm^{-2} Pt at 0.9 V.[29,31] Strasser and his group studied the composition effect of octahedral Pt–Ni nanoparticles on the ORR property and found that 11 nm-$Pt_{1.5}Ni$ was more active than 12 nm-PtNi and 13 nm-$PtNi_{1.5}$.[24] Carpenter *et al.* suggested that octahedral PtNi particles had the optimal composition for ORR among all their synthesized samples, with compositions ranging from Pt_3Ni to $PtNi_2$.[32] The inconsistencies in these studies could possibly be caused by a strong particle size effect, which has been discovered with pure Pt ORR catalyst.[5] However, to date, the relationship between the octahedral Pt–Ni alloy particle size and the ORR property has not been well studied. This is because the octahedral Pt–Ni prepared using wet synthetic methods often has both an altered particle size and composition, which interfere with each other in affecting the catalytic property.[33–37] A good method capable of separately controlling the two parameters of octahedral Pt–Ni is therefore desirable for studying the particle size effect on the ORR property.

We have recently developed a solid-state chemistry method for preparing octahedral Pt–Ni alloy nanoparticles on carbon supports (Pt–Ni/C),[4] which has proved effective in separate control of particle composition and size. Moreover, the method avoids the use of any organic capping agents and thus

Department of Chemical and Biomolecular Engineering, University of Akron, Akron, OH 44325, USA. E-mail: zpeng@uakron.edu

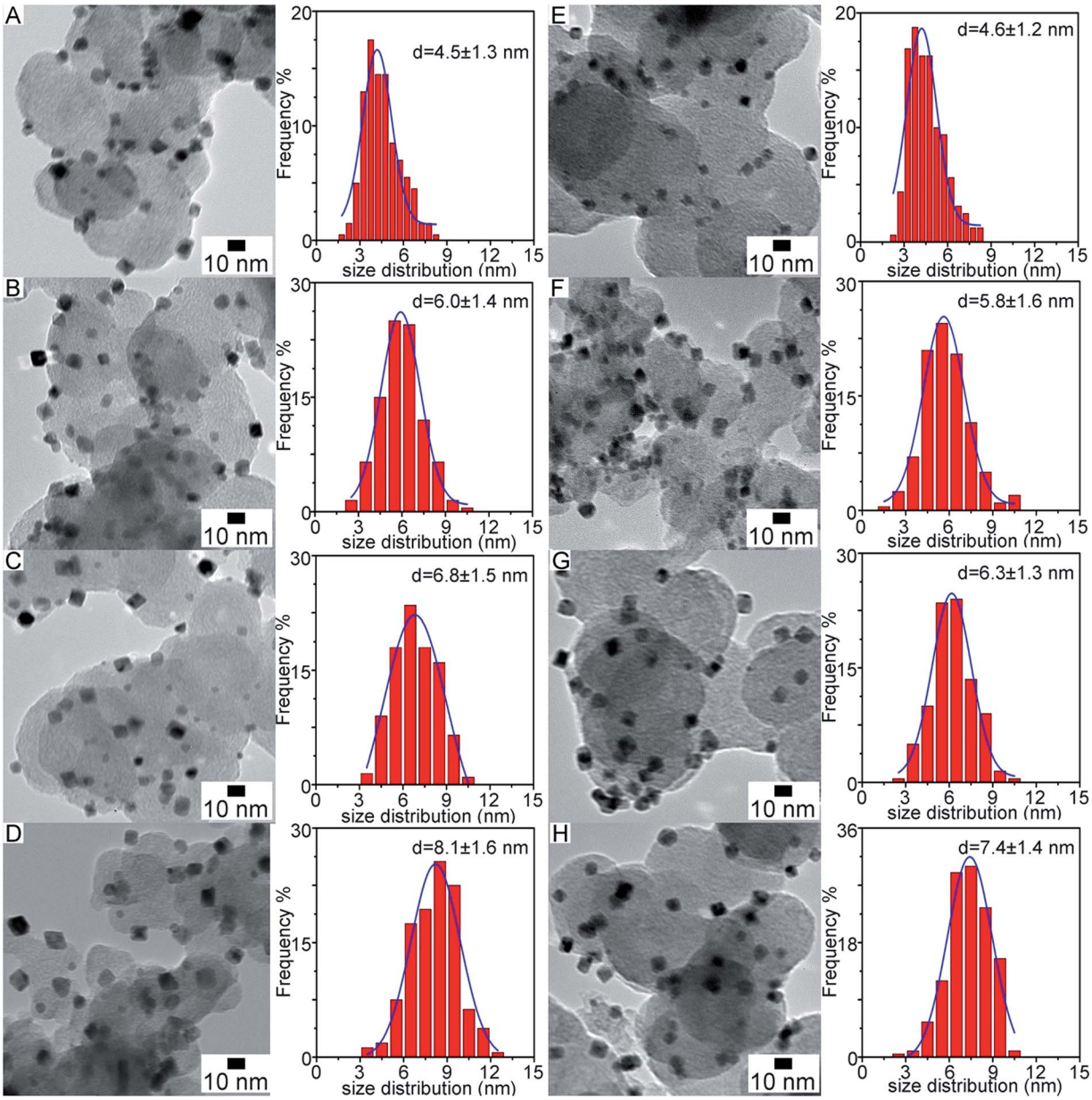

Fig. 1 TEM images of octahedral Pt–Ni/C nanoparticles prepared at different ramping rates and the particle size distribution histograms. (A–D) Pt_3Ni/C prepared at 10, 5, 2 and 1 °C min^{-1}, respectively. (E–H) $Pt_{1.5}Ni$/C prepared at 10, 5, 2 and 1 °C min^{-1}, respectively.

eliminates contamination problems of the as-prepared particles, which is crucial for accurate measurements of the intrinsic catalytic property. In this work, we prepared both octahedral Pt_3Ni/C and $Pt_{1.5}Ni$/C of different particle sizes, ranging from around 4 to 8 nm, by adjusting the synthetic parameters. The catalytic properties, including the ORR activity and catalyst stability, of the two group samples were studied, which exhibit different dependencies over the particle size. The results, in combination with characterization of fresh, activated and reacted catalysts, should provide new insights into the roles of particle size and composition of octahedral Pt–Ni on the ORR property.

Results and discussion

Both octahedral Pt_3Ni and $Pt_{1.5}Ni$ on C support (Pt_3Ni/C and $Pt_{1.5}Ni$/C) with different particle sizes were prepared by adjusting the ramp rate when the precursors were heated to 200 °C and maintained at this temperature for 1 h in H_2/CO (5/120 cm^3 min^{-1}) for reduction (Fig. 1). The majority of the Pt–Ni nanoparticles produced using the solid-state chemistry method were octahedron-shaped, with the particles dispersing uniformly on the C support and having a narrow size distribution. By using different ramp rates of 10, 5, 2, and 1 °C min^{-1} and meanwhile keeping all other parameters unchanged during the synthesis, the average edge size of the produced octahedral Pt_3Ni/C

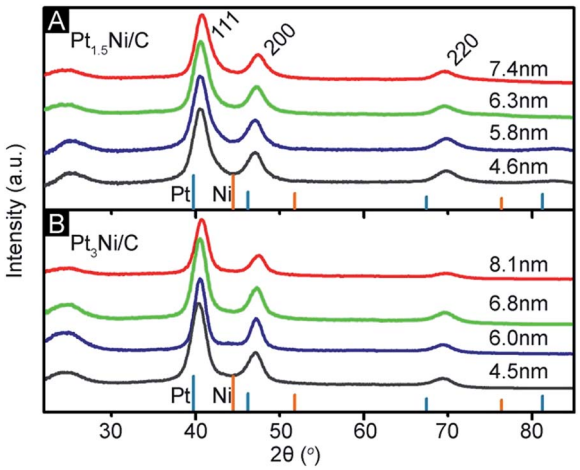

Fig. 2 Powder XRD patterns of octahedral (A) $Pt_{1.5}Ni/C$ and (B) Pt_3Ni/C with different particle sizes. Reference peaks for fcc Pt (PDF #702431) and fcc Ni (PDF #040850) are included for comparison.

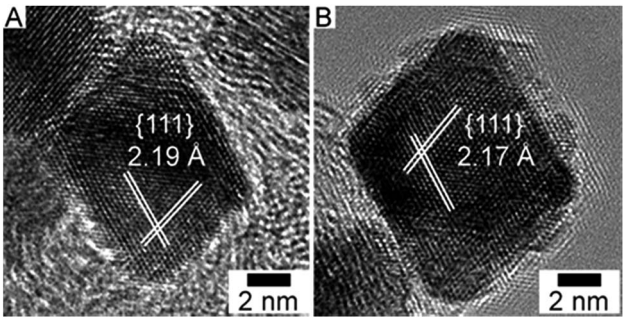

Fig. 3 HRTEM images of freshly prepared octahedral (A) Pt_3Ni and (B) $Pt_{1.5}Ni$ nanoparticles.

monotonously increased from 4.5 ± 1.3 to 6.0 ± 1.4, 6.8 ± 1.5, and finally 8.1 ± 1.6 nm from statistical analyses of over 190 particles for each sample (Fig. 1A–D). Similarly, octahedral $Pt_{1.5}Ni/C$ nanoparticles with an average edge size of 4.6 ± 1.2, 5.8 ± 1.6, 6.3 ± 1.3, and 7.4 ± 1.4 nm were obtained when the ramp rate was decreased from 10 to 1 °C min^{-1} (Fig. 1E–H). The increase in particles size with a slower ramp rate could be the result of the interplay between particle nucleation and growth kinetics.[38,39]

The octahedral Pt–Ni/C samples were characterized using powder X-ray diffraction (PXRD) for structural information (Fig. 2). The diffraction peak centered at 24.9° was attributed to the C support. Three other peaks can be indexed to (111), (200), and (220) planes of a face-centered cubic (fcc) structure. The peaks are located between those for pure Pt (PCPDFWIN #70-2431) and Ni (PCPDFWIN #040-850), confirming an alloy phase of the Pt–Ni. Compared to the octahedral Pt_3Ni/C, the diffraction peaks of the octahedral $Pt_{1.5}Ni/C$ samples had more shifts towards Ni. The increase in the peak positions were consistent with a higher Ni content in $Pt_{1.5}Ni$, as suggested by Vegard's law.[40] The samples prepared with a slower ramp rate showed a narrower full width at half maximum (FWHM) of the diffraction peaks, which indicates larger particles and agrees with the TEM observations.

Fig. 3 shows the HRTEM of Pt_3Ni and $Pt_{1.5}Ni$ nanoparticles, both of which exhibit straight edges and clear lattice fringes. The average inner plane distances (*d*-spacing) for adjacent fringes were measured to be 2.19 and 2.17 Å, which is significantly smaller than 2.27 Å for *fcc* Pt (111) and confirms the alloy formation.[29] The smaller *d*-spacing for $Pt_{1.5}Ni$ than that for Pt_3Ni is caused by a higher Ni content and agrees with the PXRD data. The samples were also characterized by energy dispersive X-ray spectroscopy (EDX) and thermal gravity analyses (TG) for determining the particles composition and metal loading, given in Table 1.

The electrochemical properties of octahedral Pt_3Ni/C with different particle sizes are shown in Fig. 4 and summarized in Table 2. Fig. 4A shows cyclic voltammograms (CV) of the activated catalysts collected in N_2-protected 0.1 M $HClO_4$. All four samples exhibit characteristic hydrogen adsorption–desorption (HAD, $\sim 0.05 < E < 0.4$ V *vs.* RHE) features, suggesting a Pt surface.[41] The ORR activity of the catalysts were measured by conducting linear sweep voltammetry (LSV) in O_2-saturated 0.1 M $HClO_4$ (Fig. 4B). The half-wave potential shifted positively with an increase in the octahedral Pt_3Ni/C particle size, indicating larger particles are more ORR active. The area-specific kinetic current density ($i_{area,0}$) of the activated catalysts at 0.90 V *vs.* RHE was obtained by applying the Koutecky–Levich equation and normalizing using their electrochemically active surface areas (ECSAs) (Fig. 4C).[42] The determined $i_{area,0}$ value was 2.47 mA cm^{-2} Pt for the 4.5 nm-Pt_3Ni/C, which further increased with the particle size. The 8.1 nm-Pt_3Ni/C exhibited the highest

Table 1 Product information of the as-prepared octahedral Pt–Ni/C alloy nanoparticles

Samples	Ramp rate (°C min^{-1})	Particle size (nm)	Pt at.% in Pt–Ni Particles	Ni at.% in Pt–Ni particles	Pt wt% in Pt–Ni/C
4.5 nm-Pt_3Ni/C	10	4.5 ± 1.3	77.31	22.69	19.03
6.0 nm-Pt_3Ni/C	5	6.0 ± 1.4	76.58	23.42	18.85
6.8 nm-Pt_3Ni/C	2	6.8 ± 1.5	78.19	21.81	18.83
8.1 nm-Pt_3Ni/C	1	8.1 ± 1.6	78.30	21.70	18.51
4.6 nm-$Pt_{1.5}Ni/C$	10	4.6 ± 1.2	60.47	39.53	19.04
5.8 nm-$Pt_{1.5}Ni/C$	5	5.8 ± 1.6	60.43	39.57	18.79
6.3 nm-$Pt_{1.5}Ni/C$	2	6.3 ± 1.4	60.86	39.14	18.56
7.4 nm-$Pt_{1.5}Ni/C$	1	7.4 ± 1.4	61.03	38.97	18.33

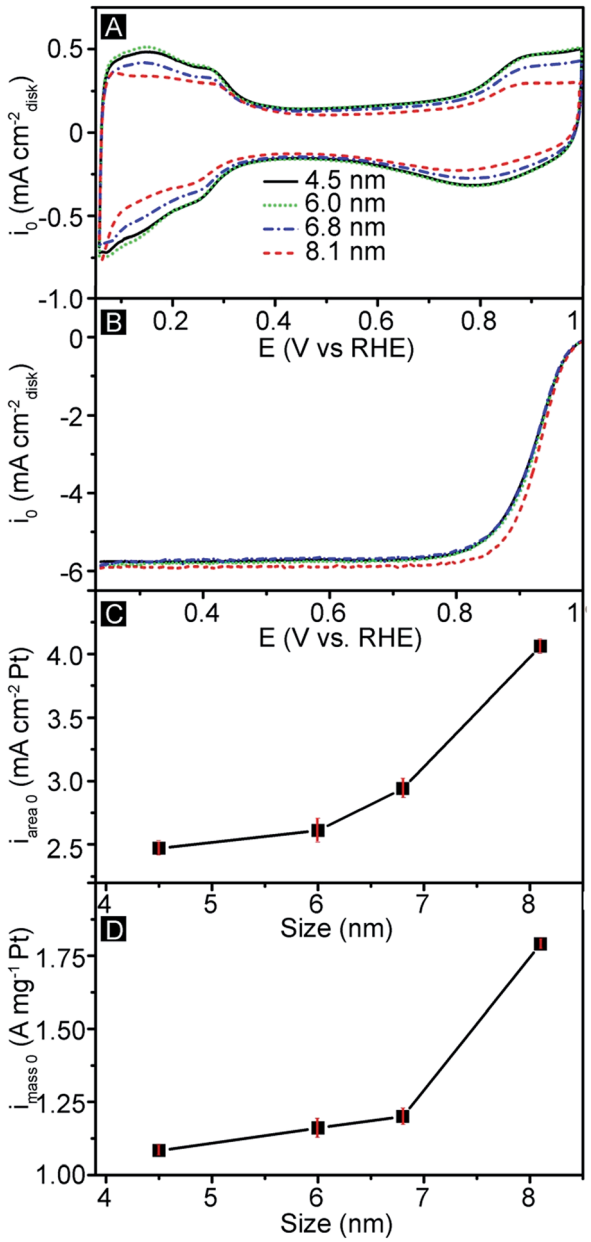

Fig. 4 (A) Cyclic voltammograms in N_2-protected 0.1 M $HClO_4$ and (B) ORR polarization curves in O_2-saturated 0.1 M $HClO_4$ of the activated octahedral Pt_3Ni/C with different particle size, and the ORR (C) area-specific current density, $i_{area,0}$, and (D) mass-specific current density, $i_{mass,0}$, at 0.9 V *vs.* RHE. All tests were repeated three times, with a standard measurement error of ±10%.

$i_{area,0}$ of 4.06 mA cm^{-2} Pt, which is more than 60% higher than that of the 4.5 nm-Pt_3Ni/C. This indicates that the 8.1 nm-Pt_3Ni/C is the most active ORR catalyst among the four octahedral Pt_3Ni/C samples. The value represents a 20-fold enhancement in the intrinsic ORR activity compared to the commercial Pt/C (0.20 mA cm^{-2} Pt) tested in our previous study.[4] The mass-specific current density ($i_{mass,0}$) of the activated octahedral Pt_3Ni/C, which is a more significant descriptor for real applications, followed a similar size dependency (Fig. 4D). The highest $i_{mass,0}$ was obtained using the 8.1 nm-Pt_3Ni/C and was 1.79 A mg^{-1} Pt, which is more than 9 times that of the commercial Pt/C, 0.196 A mg^{-1} Pt.[4]

The octahedral $Pt_{1.5}Ni$/C samples were also tested under the same condition as for the octahedral Pt_3Ni/C to study the ORR property (Fig. 5 and Table 2). Similar to the octahedral Pt_3Ni/C, all four samples exhibited characteristic HAD features and thus indicated Pt on the surface (Fig. 5A).[41] Fig. 5B shows their corresponding ORR polarization curves, which have more positive half-wave potentials compared to the octahedral Pt_3Ni/C. The observations suggest the octahedral $Pt_{1.5}Ni$/C samples are intrinsically more ORR active, which was confirmed by the calculated $i_{area,0}$ values (Fig. 5C). All four samples exhibited higher $i_{area,0}$ values than those for the octahedral Pt_3Ni/C. Meanwhile, the octahedral $Pt_{1.5}Ni$/C showed a different $i_{area,0}$-particle size relationship compared to the octahedral Pt_3Ni/C. Rather than having a monotonous increase in the ORR activity with particle size, a volcano plot was observed for the octahedral $Pt_{1.5}Ni$/C. The 4.6 nm-$Pt_{1.5}Ni$/C showed 4.57 mA cm^{-2} Pt, which increased to 4.83 mA cm^{-2} Pt when using 5.8 nm-$Pt_{1.5}Ni$/C. The $i_{area,0}$ values then decreased with further increase in the particle size, with 4.46 and 4.18 mA cm^{-2} Pt being measured for the 6.3 nm- and 7.4 nm-$Pt_{1.5}Ni$/C, respectively. It needs to be noted that the particle size-caused $i_{area,0}$ difference of the octahedral $Pt_{1.5}Ni$/C is only 15 percent at maximum, which is less significant than that for the octahedral Pt_3Ni/C and merely out of electrochemical measurement error range. The highest $i_{mass,0}$ of 2.32 A mg^{-1} Pt was also found with 5.8 nm-$Pt_{1.5}Ni$/C, suggesting the sample has the optimal particle size. Again, even the least active 7.4 nm-$Pt_{1.5}Ni$/C exhibits higher $i_{mass,0}$ than the most active 8.1 nm-Pt_3Ni/C, suggesting $Pt_{1.5}Ni$ has a more optimal particle composition for ORR. By using the optimal 5.8 nm-$Pt_{1.5}Ni$/C, the $i_{area,0}$ and $i_{mass,0}$ values are about 24 and 12 times those of using the commercial Pt/C.[4]

The long-term stability of the octahedral Pt–Ni/C was investigated by applying linear potential sweeps between 0.60 and 1.00 V *vs.* RHE at 50 mV s^{-1} for 4000 cycles and measuring changes in the electrochemical property (Fig. 6 and Table 2). The ECSA loss for the octahedral Pt_3Ni/C seems not strongly size-dependent, with a value of about 8% observed for all four samples (Fig. 6A). The good ECSA retention suggests no dramatic change in the octahedral Pt_3Ni particle size during the stability test. Despite the small ECSA changes, the ORR activity decreased dramatically (Fig. 6B). The 4.5 nm-Pt_3Ni/C exhibited 1.24 mA cm^{-2} Pt after the stability test, which represents a 50% loss in the i_{area} compared to the fresh counterpart. The catalyst stability barely changed with the particle size, with the 8.1 nm-Pt_3Ni/C retaining 52% of its initial activity. As a result of both ECSA loss and i_{area} decrease, the octahedral Pt_3Ni/C samples had large drops in the mass-specific ORR activity (Fig. 6C). The after-test i_{mass} decreased by 51% even for the best performing 8.1 nm-Pt_3Ni/C. The stability of the octahedral $Pt_{1.5}Ni$/C samples, however, showed a different size dependency. The ECSA loss for both 4.6 nm- and 5.8 nm-$Pt_{1.5}Ni$/C was about 2%, which is even less than the loss for the octahedral Pt_3Ni/C. However, a further increase in the particle size caused more severe instability and larger ECSA losses. The 6.3 nm-$Pt_{1.5}Ni$/C had an initial ECSA value of 41.57 m^2 g^{-1} Pt, which dropped by

Table 2 Electrochemical properties of the octahedral Pt–Ni/C before and after the stability test

	Freshly activated catalyst			Catalyst after stability test		
Samples	$ECSA_0$ ($m^2\ g^{-1}$ Pt)	$i_{area,0}$ (mA cm^{-2} Pt)	$i_{mass,0}$ (A mg^{-1} Pt)	ECSA ($m^2\ g^{-1}$ Pt)	i_{area} (mA cm^{-2} Pt)	i_{mass} (A mg^{-1} Pt)
4.5 nm-Pt_3Ni/C	41.67	2.47	1.08	38.26	1.24	0.50
6.0 nm-Pt_3Ni/C	42.55	2.61	1.18	39.23	1.31	0.55
6.8 nm-Pt_3Ni/C	35.86	2.94	1.20	33.1	1.5	0.58
8.1 nm-Pt_3Ni/C	34.16	4.06	1.79	31.66	2.11	0.87
4.6 nm-$Pt_{1.5}Ni$/C	46.95	4.57	2.28	45.98	1.98	0.97
5.8 nm-$Pt_{1.5}Ni$/C	45.81	4.83	2.32	45.24	2.16	1.03
6.3 nm-$Pt_{1.5}Ni$/C	41.57	4.46	2.11	36.33	1.96	0.88
7.4 nm-$Pt_{1.5}Ni$/C	37.77	4.18	1.82	31.81	1.77	0.65

13% to 36.33 $m^2\ g^{-1}$ Pt after the stability test. The 7.4 nm-$Pt_{1.5}Ni$/C showed an even poorer ECSA stability, with about 16% loss. Additionally, the reacted samples had comparable losses in the i_{area}, ranging from 55% for the 5.8 nm-$Pt_{1.5}Ni$/C to 58% for the 7.4 nm-$Pt_{1.5}Ni$/C. The 5.8 nm-$Pt_{1.5}Ni$/C was found to have the least loss in the i_{mass} among all four samples, with 44% of the activity being retained after the stability test. The 7.4 nm-$Pt_{1.5}Ni$/C exhibited the biggest loss and retained only 36% of the initial activity.

TEM characterizations of the after-test Pt_3Ni/C showed no significant change in the particle size (Fig. 7A), which was consistent with the small ECSA drop during the accelerated stability test. This observation indicates little agglomeration or sintering of the Pt_3Ni particles over the course of testing. However, the majority of the particles lost their octahedral morphology. Fig. 7B shows the HRTEM of one individual reacted Pt_3Ni particle, the sharp corners and edges of which became more rounded compared to the fresh Pt_3Ni. Similar results were found for the reacted octahedral $Pt_{1.5}Ni$/C, which experienced little change in the particle size but significant variation in the particle morphology (Fig. 7C and D). An interesting observation is that some of the reacted $Pt_{1.5}Ni$ maintained an octahedral skeleton and became concave in the facets, which could be as a result of significant Ni leaching from the facet center. Similar observations have been reported by Strasser and collaborators.[24,34] They found Ni was rich in the surface and Pt was rich in the edges and corners of fresh octahedral $Pt_{1.5}Ni$ nanoparticles, which formed concave octahedrons during the stability test.[24,34]

The compositions of the fresh, activated and reacted Pt–Ni/C were determined using EDX quantitative analyses and shown for comparison in Fig. 8. The Ni contents in both fresh Pt_3Ni/C and $Pt_{1.5}Ni$/C were close to the amounts of metal precursors, which validate high efficiency of the solid-state chemistry method in making octahedral Pt–Ni/C with precise composition-control. Significant decreases in the Ni contents were observed for the activated samples and suggested rapid Ni loss during the activation process, probably due to fast dissolution of Ni in the near surface layers and formation of a pure Pt surface.[24,34] The reacted Pt_3Ni/C samples showed further decrease in the Ni content compared to their activated counterparts, confirming Ni leaching during the stability test. The final composition of the reacted Pt_3Ni/C was found to be independent of the particle size and was determined to be around $Pt_{82}Ni_{18}$, which could account for the large drop in the ORR activity during the stability test and the small dependency of ORR stability on the particle size.[24,43] The composition change means 30% of the Ni atoms in the fresh particles leach out during the activation process and the stability test. The octahedral $Pt_{1.5}Ni$ experienced more and size-dependent Ni leaching compared to the octahedral Pt_3Ni. The final composition of reacted 4.6 nm-$Pt_{1.5}Ni$/C is $Pt_{82}Ni_{18}$, indicating that around 67% of the Ni leached out. The larger $Pt_{1.5}Ni$ particles were less stable and had more Ni leaching compared to the smaller ones. The composition of 7.4 nm-$Pt_{1.5}Ni$ changed to $Pt_{86}Ni_{14}$ after the test, which indicates a loss of 77% of the Ni atoms. Fig. 8C–E shows the STEM and EDX line scans of the fresh, activated, and after-test octahedral Pt_3Ni nanoparticles. Both Pt and Ni elements were found throughout the fresh particles, with both elements present in the particle surfaces. A gap between Pt and Ni signals was observed immediately after activation of the particles, indicating that Ni quickly begins to leach out and a pure Pt surface forms during the activation process. These results agreed well with the CV curves of the activated Pt_3Ni/C, which show the characteristic HAD features of the Pt surface. The particles after the stability test still contained both elements. However compared to the activated ones, the gap between the Pt and Ni signals became even broader and the Ni signals were weaker, suggesting more leaching of Ni and the thickening of the Pt surface layers. Similar observations were also found with the octahedral $Pt_{1.5}Ni$ nanoparticles.

Alloying with 3d transition metals has been proved to be an effective strategy for improving the electrocatalytic property of Pt in many cases. The much higher ORR activity of octahedral Pt–Ni nanoparticles than pure Pt has been attributed to their altered electronic and geometric structure.[1,44] The working octahedral Pt–Ni nanoparticles have a closely-packed pure Pt (111) surface, because surface Ni readily dissolves in acid and under potential.[24,45] The surface layer of the octahedral Pt–Ni has a down-shifted ε_d compared to pure Pt, which has been attributed to the electronic interaction between Ni in sublayers and surface Pt. The down shift in ε_d could effectively weaken the bond strength between surface Pt atoms and oxygenated species and yield promoted ORR kinetics.[44] It needs to be noted that the octahedral $Pt_{1.5}Ni$ nanoparticles were found to be more ORR

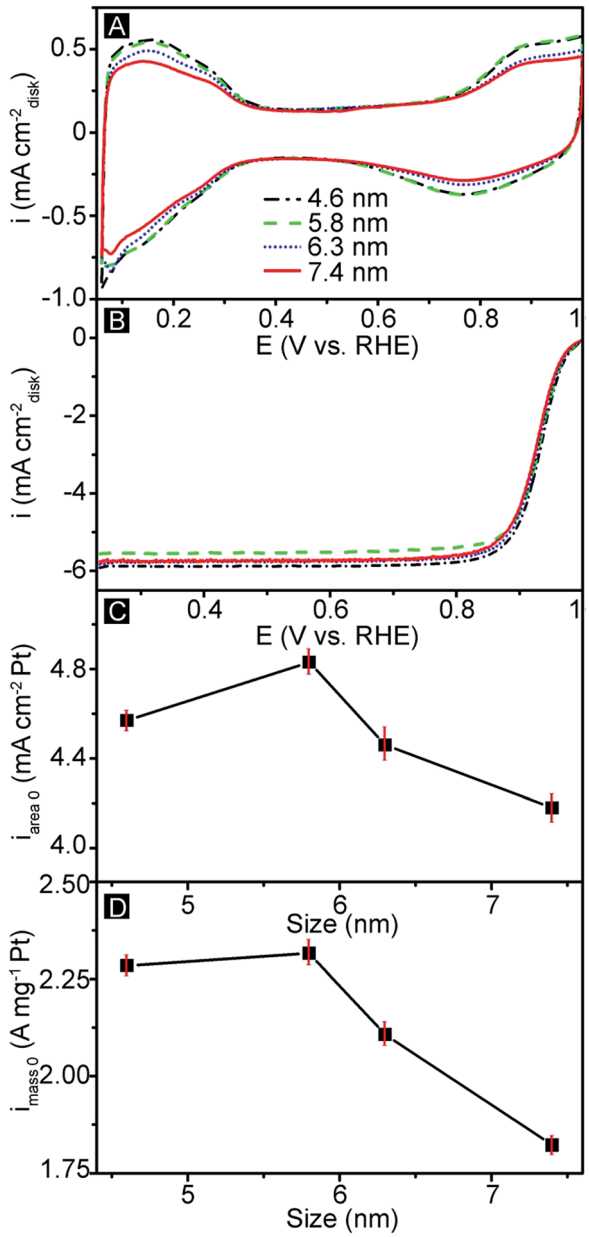

Fig. 5 (A) Cyclic voltammograms in N_2-protected 0.1 M $HClO_4$ and (B) ORR polarization curves in O_2-saturated 0.1 M $HClO_4$ of the activated octahedral $Pt_{1.5}Ni$/C with different particle size, and the ORR (C) area-specific current density, $i_{area,0}$, and (D) mass-specific current density, $i_{mass,0}$, at 0.9 V *vs.* RHE. All tests were repeated three times, with a standard measurement error of ±10%.

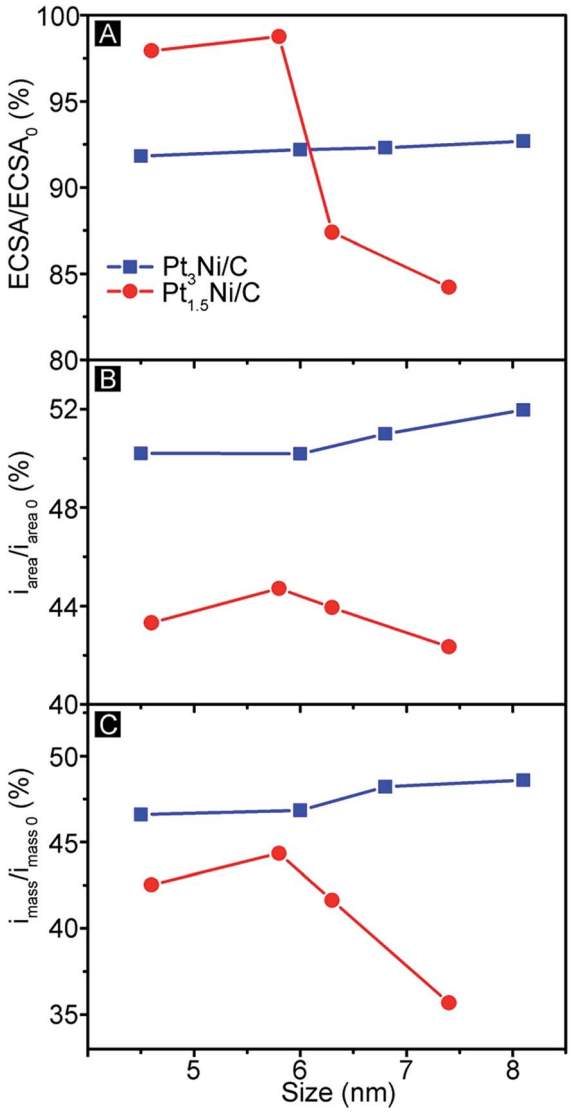

Fig. 6 The changes in (A) ECSA, (B) i_{area}, and (C) i_{mass} of the octahedral Pt_3Ni/C and $Pt_{1.5}Ni$/C after stability test with respect to that for the activated counterparts. The accelerated stability test includes 4000 potential cycles between 0.60 and 1.0 V *vs.* RHE at 50 mV s^{-1} in N_2-protected 0.1 M $HClO_4$.

active than the octahedral Pt_3Ni particles in the research, whereas previous study on single crystals suggests the highest activity of Pt_3Ni (111).[1] The discrepancy in the optimal catalyst composition between the nanoparticle and the bulk Pt–Ni has also been reported in previous studies.[24,29,31,32] It could be associated with the difference in their elemental distribution. The Ni was found rich in content in the surface layers of the octahedral Pt–Ni nanoparticles, which is dissimilar to its uniform distribution in the bulk Pt–Ni (111) and could affect the electronic structure of surface Pt. The octahedral $Pt_{1.5}Ni$ nanoparticles might have a more optimal ε_d value than the octahedral Pt_3Ni and thus possess more activity.

The size dependency of the ORR property of the octahedral Pt–Ni particles could also be related to their electronic and geometric structure. The monotonous increase in the ORR activity with size of the octahedral Pt_3Ni could be associated with an increase in the fraction of (111) terraces.[46] The smaller particles have more edge and corner Pt atoms on the surface, which have a stronger adsorption of oxygenated species than terrace Pt and negatively influence the ORR kinetics. The large loss in the ORR activity during the accelerated stability test is possibly caused by gradual Ni leaching, which leads to thickened and possibly restructured Pt surface layers, up-shifts in ε_d compared to the fresh octahedral Pt_3Ni, and consequently decreased reaction kinetics.[24] Interestingly, the Ni loss during the test was found almost independent of the octahedral Pt_3Ni

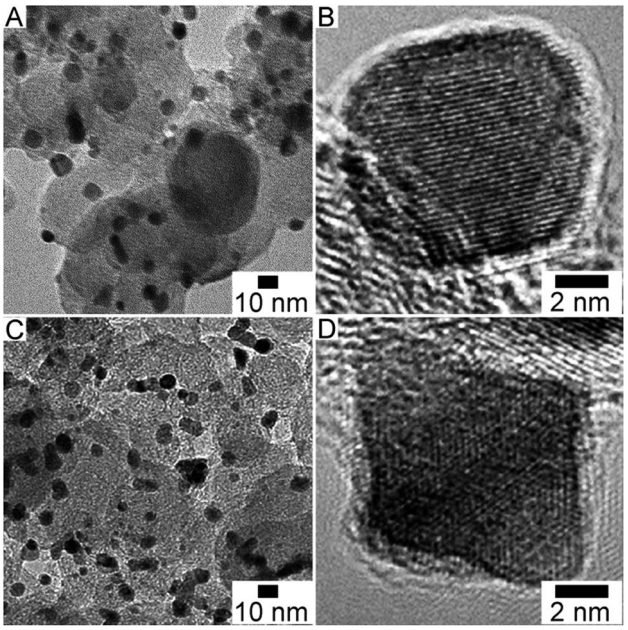

Fig. 7 TEM and HRTEM images of the (A and B) Pt_3Ni/C and (C and D) $Pt_{1.5}Ni/C$ after the stability test.

size, which could account for the small size dependency of the catalyst stability. In comparison, the volcano-type relationship obtained for both ORR activity and catalyst stability of the octahedral $Pt_{1.5}Ni$ over the particle size could be the result of a complex interplay between a size-dependent Ni leaching process and (111) terraces.[9,24,33,34,45] On one side, an increase in the particle size can improve the fraction of (111) terraces, which has a positive effect on the ORR kinetics. On the other side, the high Ni content in the fresh octahedral $Pt_{1.5}Ni$ nanoparticles and its inhomogeneous distribution can cause a rapid leaching process in both catalyst activation and stability test, as evidenced by the EDX data.[45] The larger particles have a faster Ni leaching rate, which negatively influences the ORR kinetics. The two size effects compete with each other, leading to the 5.8 nm-$Pt_{1.5}Ni$ being the most active and stable catalyst. Meanwhile, the faster Ni leaching process compared to that of the octahedral Pt_3Ni results in less stability of the octahedral $Pt_{1.5}Ni$.

Conclusions

Both octahedral Pt_3Ni/C and $Pt_{1.5}Ni/C$ with particle sizes ranging from about 4 to 8 nm were prepared using a solid-state chemistry method, which was surfactant-free and enabled the separate control of particle size and composition. The octahedral Pt_3Ni/C exhibited a monotonous increase in the ORR activity with a particle size, with 2.47 mA cm^{-2} Pt for the 4.5 nm-Pt_3Ni/C and 4.06 mA cm^{-2} Pt for the 8.1 nm-Pt_3Ni/C at 0.9 V *vs.* RHE. The significantly size-varied ORR activity was attributed to the change in the fraction of (111) terraces, which is size-dependent. The Pt_3Ni/C showed a small dependency of catalyst stability on the particle size, with about 30% loss of Ni and a 50% drop in the ORR activity during the stability test for all

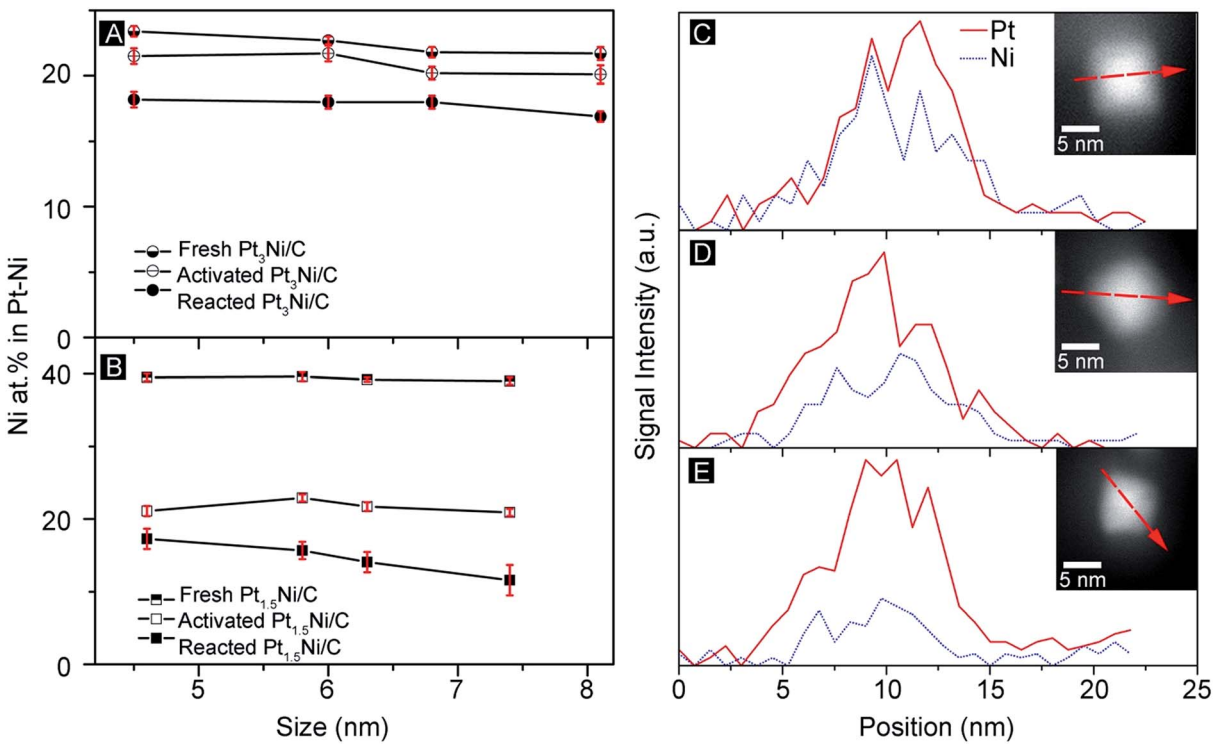

Fig. 8 Ni content in the fresh and after-stability-test octahedral (A) Pt_3Ni/C and (B) $Pt_{1.5}Ni/C$ nanoparticles, and EDX line scans of (C) freshly prepared, (D) activated, and (E) after-stability-test octahedral Pt_3Ni nanoparticles. STEM insets show the individual particles and scan directions for the EDX elemental analyses.

samples. In comparison, the octahedral $Pt_{1.5}Ni$/C exhibited a different size dependency of the ORR activity, Ni loss, and catalyst stability. The 5.8 nm-$Pt_{1.5}Ni$/C performed best among all four catalysts, with the highest initial activity of 4.83 mA cm^{-2} Pt and the least 55% drop in i_{area} after the stability test. The larger $Pt_{1.5}Ni$ showed a faster Ni leaching rate, with around 67% Ni loss for the 4.6 nm-$Pt_{1.5}Ni$/C and 77% Ni loss for the 7.4 nm-$Pt_{1.5}Ni$/C during the stability test. The volcano relationship between the ORR activity and the $Pt_{1.5}Ni$ size could be caused by the interplay between less stability and a higher fraction of (111) terraces of the larger octahedral $Pt_{1.5}Ni$ particles. We believe the findings will spark more research into establishing accurate size-intrinsic property relationships and improving the activity and stability of noble metal alloy catalysts for practical applications.

Experimental

Materials

Platinum acetylacetonate ($Pt(acac)_2$, 97%) and nickel acetylacetonate ($Ni(acac)_2$, 95%) were purchased from Sigma-Aldrich. Acetone (C_3H_6O, 99.8%) and anhydrous ethanol (ETOH, 95.3%) were from Fisher Scientific. Concentrated perchloric acid ($HClO_4$, 70%) was from JT Baker. Carbon support (C, Vulcan® XC-72R) was purchased from Cabot. Commercial Pt/C (HP 20 wt% Pt) was purchased from fuel cell store. Hydrogen (H_2, 99.999%), carbon monoxide (CO, 99.999%), oxygen (O_2, 999.99%) and nitrogen (N_2, 99.999%) gases were obtained from Praxair.

Preparation of octahedral Pt–Ni/C

The octahedral Pt–Ni/C nanoparticles were prepared using a solid-state chemistry method,[4] which involved impregnation of both metal precursors on a C support and reducing them in CO and H_2 gas mixture. Typically, for preparing octahedral Pt_3Ni/C (20 wt% Pt), C was thermally treated in air at 300 °C overnight for removal of moisture prior to use. $Pt(acac)_2$ (40 mg or 0.1 mmol) and $Ni(acac)_2$ (8.6 mg or 0.033 mmol) were first dissolved in acetone (3 mL), and then added dropwise onto the pretreated C support (80 mg) under vigorous stirring. After impregnation, the mixture was immediately transferred to a furnace which was purged by N_2 flow for 20 minutes. The mixtures were reduced by heating at a designated ramping rate to 200 °C and maintaining at that temperature for 1 hour in H_2/CO (5/120 cm^3 min^{-1}). The gas atmosphere was switched back to N_2 and the product was cooled down to room temperature after the reaction. The samples were collected and stored in N_2 for characterization and testing. The octahedral $Pt_{1.5}Ni$/C were prepared using a similar procedure but with different amounts of $Pt(acac)_2$ and $Ni(acac)_2$ precursors. The particle size of the octahedral Pt–Ni/C was tuned by adjusting the ramping rate and meanwhile keeping all other synthetic parameters the same.

Characterization

Transmission electron microscopy (TEM) images of the prepared Pt–Ni/C samples were characterized by a JEOL JEM-1230 microscope operated at 120 kV. High-resolution TEM (HRTEM), high-angle annular dark field scanning TEM (HAADF-STEM), and energy dispersive X-ray (EDX) elemental line scans of individual Pt–Ni nanoparticles were taken using a FEI Tecnai G2 F20 microscope operated at 200 kV. The X-ray diffraction (XRD) patterns were recorded on a Bruker AXS Dimension D8 X-ray diffractometer with Cu Kα radiation source. Composition analysis of the as-prepared Pt–Ni catalysts were conducted using EDX equipped with a JEOL-7401 field emission scanning electron microscope (FESEM) with an operating voltage at 25 kV. The accurate metal loading of Pt–Ni/C products was determined by heating the samples at 10 °C min^{-1} to 750 °C in a flow of air (60 cm^3 min^{-1}) and measuring the weight of residue in a thermal gravimetric instrument (TA Instruments, Model Q50).

Rotating disk electrode (RDE) catalyst film preparation

Thin catalyst films were drop-casted onto RDE for the electrochemical study. In a typical procedure for preparing the films, catalyst ink (1 mg catalyst per mL) was prepared by mixing sample powders with a stock solution containing DI water, isopropanol, and Nafion ionomer ($V_{water} : V_{iso\text{-}propanol} : V_{5\%\ Nafion} = 0.8 : 0.2 : 0.005$) and sonicating for 20 min. A glassy carbon electrode (5 mm in diameter) was polished by using a 0.05 μm alumina-particle suspension (Buehler) and rinsing with Millipore ultrapure DI water, which was followed by 2 min sonication and rinsing with DI water three times. 10 μL fresh ink was transferred onto the glassy carbon electrode after 20 seconds of sonication. The electrode was mounted on to a home-made electrode rotator and was rotated at a speed of 500 rpm for around 20 min, which allowed the formation of uniform thin catalyst films.[47]

Electrochemical measurements

The electrochemical experiments were conducted using a CHI 760D electrochemical workstation (CH Instruments, Inc.) and a rotating disk electrode controller (AFMSRCE, Pine Instrument Co.). A three-electrode system, consisting of the catalyst film-coated glassy carbon working electrode, a platinum wire counter electrode, and a HydroFlex reference electrode (ET070, Edaq Inc.), were used for all electrochemical measurements. The reference electrode was placed in one separate beaker and was connected to the reaction cell with a bridge tube. The reaction cell, the bridge tube and the beaker were filled with the same electrolyte. Solution resistance of the testing system was determined by electrochemical impedance spectroscopy (EIS). The potentials of the reference electrode were calibrated using a home-built reversible hydrogen electrode (RHE). All the potentials were recorded with respect to the HydroFlex electrode and were reported with respect to RHE.

The measurement of electrochemical active surface area (ECSA) of the catalysts was conducted in an N_2-protected 0.1 M $HClO_4$ aqueous solution at room temperature. The catalysts were first activated by sweeping in the potential range of 0.05–1.00 V *vs.* RHE at a scan rate of 100 mV s^{-1} for 25 cycles to yield stable CV curves, which was followed by a few more CV cycles

using the same potential and scan parameters. The ECSA values of the catalysts were calculated by integrating the area in the hydrogen adsorption range (~0.05–0.40 V *vs.* RHE) from the backward sweep in the CV curves.

The oxygen reduction reaction (ORR) property of the octahedral Pt–Ni/C catalysts was studied using linear sweep voltammetry (LSV). The potential was swept from 0.2 V to 1.0 V at a scan rate of 10 mV s^{-1} and an electrode rotation rate of 1600 rpm in O_2-saturated 0.1 M $HClO_4$ aqueous solution. The kinetic currents (I_k), which represent the intrinsic ORR activity of the catalysts, were calculated using the Koutecky–Levich equation:[25]

$$\frac{1}{I} = \frac{1}{I_k} + \frac{1}{B\omega^{1/2}} \quad (1)$$

where I is the measured current, B is a constant and ω is the angular rotating frequency of the working electrode ($\omega = 2\pi f/60$, f is the RDE rotation rate in rpm). The ohmic *iR* drop during the ORR experiments was corrected for accurate measurement of the intrinsic ORR property.[48] The stability of the octahedral Pt–Ni/C was studied using an accelerated stability test, in which repetitive CV scans were performed between 0.60 and 1.00 V *vs.* RHE at a scan rate of 50 mV s^{-1} for 4000 cycles in N_2-protected 0.1 M $HClO_4$. Prior to any stability test, the catalyst loaded electrode was cycled between 0.05 and 1.00 V at a scan rate of 100 mV s^{-1} 50 times. After the 4000-cycle scan in N_2-saturated solution, 300 cycles of CV scan at 10 V s^{-1} between 0–1.00 V *vs.* RHE were first applied for removal of accumulated impurity cations/anions adsorbed to the catalyst surface before the ECSA and ORR activity measurements, which ensured stable and reproducible experimental results.[49]

Acknowledgements

Supported by the University of Akron start-up fund (Z. P.). The HRTEM data were obtained at the (cryo)TEM facility at the Liquid Crystal Institute, Kent State University, supported by the Ohio Research Scholars Program Research Cluster on Surfaces in Advanced Materials. The authors thank Dr Min Gao for technical support with the TEM experiments.

Notes and references

1 V. R. Stamenkovic, B. Fowler, B. S. Mun, G. Wang, P. N. Ross, C. A. Lucas and N. M. Marković, *Science*, 2007, **315**, 493.
2 P. Strasser, S. Koh, T. Anniyev, J. Greeley, K. More, C. Yu, Z. Liu, S. Kaya, D. Nordlund, H. Ogasawara, M. F. Toney and A. Nilsson, *Nat. Chem.*, 2010, **2**, 454.
3 M. K. Debe, *Nature*, 2012, **486**, 43.
4 C. Zhang, S. Y. Hwang, A. Trout and Z. Peng, *J. Am. Chem. Soc.*, 2014, **136**, 7805.
5 H. A. Gasteiger, S. S. Kocha, B. Sompalli and F. T. Wagner, *Appl. Catal., B*, 2005, **56**, 9.
6 H. A. Gasteiger and N. M. Marković, *Science*, 2009, **324**, 48.
7 J. Greeley, I. E. L. Stephens, A. S. Bondarenko, T. P. Johansson, H. A. Hansen, T. F. Jaramillo, J. Rossmeisl, I. Chorkendorff and J. K. Nørskov, *Nat. Chem.*, 2009, **1**, 552.
8 M. Oezaslan, M. Heggen and P. Strasser, *J. Am. Chem. Soc.*, 2012, **134**, 514.
9 S. Zhang, X. Zhang, G. Jiang, H. Zhu, S. Guo, D. Su, G. Lu and S. Sun, *J. Am. Chem. Soc.*, 2014, **136**, 7734.
10 C. Liang, L. Ding, C. Li, M. Pang, D. Su, W. Li and Y. Wang, *Energy Environ. Sci.*, 2010, **3**, 1121.
11 H. Jin, H. Zhang, H. Zhong and J. Zhang, *Energy Environ. Sci.*, 2011, **4**, 3389.
12 S.-T. Chang, C.-H. Wang, H.-Y. Du, H.-C. Hsu, C.-M. Kang, C.-C. Chen, J. C. S. Wu, S.-C. Yen, W.-F. Huang, L.-C. Chen, M. C. Lin and K.-H. Chen, *Energy Environ. Sci.*, 2012, **5**, 5305.
13 P. Zhang, F. Sun, Z. Xiang, Z. Shen, J. Yun and D. Cao, *Energy Environ. Sci.*, 2014, **7**, 442.
14 S. Wang, D. Yu and L. Dai, *J. Am. Chem. Soc.*, 2011, **133**, 5182.
15 Y. Chen, Z. Liang, F. Yang, Y. Liu and S. Chen, *J. Phys. Chem. C*, 2011, **115**, 24073.
16 J.-H. Jang, J. Kim, Y.-H. Lee, I. Y. Kim, M.-H. Park, C.-W. Yang, S.-J. Hwang and Y.-U. Kwon, *Energy Environ. Sci.*, 2011, **4**, 4947.
17 S. Yin, M. Cai, C. Wang and P. K. Shen, *Energy Environ. Sci.*, 2011, **4**, 558.
18 W. Zhou, J. Sunarso, Z.-G. Chen, L. Ge, J. Motuzas, J. Zou, G. Wang, A. Julbe and Z. Zhu, *Energy Environ. Sci.*, 2011, **4**, 872.
19 K. A. Kuttiyiel, K. Sasaki, Y. Choi, D. Su, P. Liu and R. R. Adzic, *Energy Environ. Sci.*, 2012, **5**, 5297.
20 J. Xu, P. Gao and T. S. Zhao, *Energy Environ. Sci.*, 2012, **5**, 5333.
21 J. Yang, X. Chen, X. Yang and J. Y. Ying, *Energy Environ. Sci.*, 2012, **5**, 8976.
22 S. Mao, Z. Wen, T. Huang, Y. Hou and J. Chen, *Energy Environ. Sci.*, 2014, **7**, 609.
23 V. Mazumder, M. Chi, K. L. More and S. Sun, *J. Am. Chem. Soc.*, 2010, **132**, 7848.
24 C. Cui, L. Gan, M. Heggen, S. Rudi and P. Strasser, *Nat. Mater.*, 2013, **12**, 765.
25 D. Wang, H. L. Xin, R. Hovden, H. Wang, Y. Yu, D. A. Muller, F. J. DiSalvo and H. D. Abruña, *Nat. Mater.*, 2013, **12**, 81.
26 C. Chen, Y. Kang, Z. Huo, Z. Zhu, W. Huang, H. L. Xin, J. D. Snyder, D. Li, J. A. Herron, M. Mavrikakis, M. Chi, K. L. More, Y. Li, N. M. Markovic, G. A. Somorjai, P. Yang and V. R. Stamenkovic, *Science*, 2014, **343**, 1339.
27 Y. Zhang, Y.-C. Hsieh, V. Volkov, D. Su, W. An, R. Si, Y. Zhu, P. Liu, J. X. Wang and R. R. Adzic, *ACS Catal.*, 2014, **4**, 738.
28 R. Yang, J. Leisch, P. Strasser and M. F. Toney, *Chem. Mater.*, 2010, **22**, 4712.
29 S.-I. Choi, S. Xie, M. Shao, J. H. Odell, N. Lu, H.-C. Peng, L. Protsailo, S. Guerrero, J. Park, X. Xia, J. Wang, M. J. Kim and Y. Xia, *Nano Lett.*, 2013, **13**, 3420.
30 C. Wang, D. van der Vliet, K.-C. Chang, H. You, D. Strmcnik, J. A. Schlueter, N. M. Markovic and V. R. Stamenkovic, *J. Phys. Chem. C*, 2009, **113**, 19365.
31 S.-I. Choi, S. Xie, M. Shao, N. Lu, S. Guerrero, J. H. Odell, J. Park, J. Wang, M. J. Kim and Y. Xia, *ChemSusChem*, 2014, **7**, 1476.
32 M. K. Carpenter, T. E. Moylan, R. S. Kukreja, M. H. Atwan and M. M. Tessema, *J. Am. Chem. Soc.*, 2012, **134**, 8535.

33 K. Jayasayee, J. A. R. V. Veen, T. G. Manivasagam, S. Celebi, E. J. M. Hensen and F. A. de Bruijn, *Appl. Catal., B*, 2012, **111–112**, 515.
34 C. Cui, L. Gan, M. Neumann, M. Heggen, B. Roldan Cuenya and P. Strasser, *J. Am. Chem. Soc.*, 2014, **136**, 4813.
35 L. Liu, G. Samjeske, S.-i. Nagamatsu, O. Sekizawa, K. Nagasawa, S. Takao, Y. Imaizumi, T. Yamamoto, T. Uruga and Y. Iwasawa, *Top. Catal.*, 2014, **57**, 595.
36 L. Zhang and Y. Xia, *Adv. Mater.*, 2014, **26**, 2600.
37 R. Loukrakpam, J. Luo, T. He, Y. Chen, Z. Xu, P. N. Njoki, B. N. Wanjala, B. Fang, D. Mott, J. Yin, J. Klar, B. Powell and C.-J. Zhong, *J. Phys. Chem. C*, 2011, **115**, 1682.
38 Z. Peng, C. Kisielowski and A. T. Bell, *Chem. Commun.*, 2012, **48**, 1854.
39 T.-T. Duong, J.-S. Choi, A.-T. Le and S.-G. Yoon, *J. Electrochem. Soc.*, 2014, **161**, H166.
40 A. R. Denton and N. W. Ashcroft, *Phys. Rev. A: At., Mol., Opt. Phys.*, 1991, **43**, 3161.
41 E. Yeager, W. E. O'Grady, M. Y. C. Woo and P. Hagans, *J. Electrochem. Soc.*, 1978, **125**, 348.
42 T. J. Schmidt, H. A. Gasteiger, G. D. Stäb, P. M. Urban, D. M. Kolb and R. J. Behm, *J. Electrochem. Soc.*, 1998, **145**, 2354.
43 S. Chen, H. A. Gasteiger, K. Hayakawa, T. Tada and Y. Shao-Horn, *J. Electrochem. Soc.*, 2010, **157**, A82.
44 V. Stamenkovic, B. S. Mun, K. J. J. Mayrhofer, P. N. Ross, N. M. Markovic, J. Rossmeisl, J. Greeley and J. K. Nørskov, *Angew. Chem., Int. Ed.*, 2006, **45**, 2897.
45 H. R. Colón-Mercado, H. Kim and B. N. Popov, *Electrochem. Commun.*, 2004, **6**, 795.
46 F. J. Perez-Alonso, D. N. McCarthy, A. Nierhoff, P. Hernandez-Fernandez, C. Strebel, I. E. L. Stephens, J. H. Nielsen and I. Chorkendorff, *Angew. Chem., Int. Ed.*, 2012, **51**, 4641.
47 Y. Garsany, I. L. Singer and K. E. Swider-Lyons, *J. Electroanal. Chem.*, 2011, **662**, 396.
48 D. v. d. Vliet, D. S. Strmcnik, C. Wang, V. R. Stamenkovic, N. M. Markovic and M. T. M. Koper, *J. Electroanal. Chem.*, 2010, **647**, 29.
49 A. Holewinski, J.-C. Idrobo and S. Linic, *Nat. Chem.*, 2014, **6**, 828.